DOI: 10.1002/cplu.201200242

Tin Oxide Nanoparticles and SnO_2/SiO_2 Hybrid Materials by Twin Polymerization Using Tin(IV) Alkoxides

Christian Leonhardt,[a] Susann Brumm,[a] Andreas Seifert,[b] Gerhard Cox,[c] Arno Lange,[c] Tobias Rüffer,[d] Dieter Schaarschmidt,[d] Heinrich Lang,[d] Nathanael Jöhrmann,[e] Michael Hietschold,[e] Frank Simon,[f] and Michael Mehring*[a]

Twin polymerization was used to prepare composite materials composed of SnO_2 nanoparticles entrapped in a polymer matrix. Novel, well-defined tin-containing molecular precursors, so-called twin monomers, were synthesized by transesterification starting from $Sn(OR)_4$ (R = *t*Bu, *t*Am) to give $Sn(OCH_2C_4H_3O)_4$ (**1**), $[Sn(OCH_2C_4H_3S)_4{\cdot}HOCH_2C_4H_3S]_2$ (**2**), $[Sn(OCH_2\text{-}2\text{-}OCH_3C_6H_4)_4{\cdot}HOCH_2\text{-}2\text{-}OCH_3C_6H_4]_2$ (**3**), $[Sn(OCH_2\text{-}2,4\text{-}(OCH_3)_2C_6H_3)_4{\cdot}HOCH_2\text{-}2,4\text{-}(OCH_3)_2C_6H_3]_2$ (**4**), 2,2′-spirobi[4*H*-1,3,2-benzodioxastannine] (**5**), 2,2′-spirobi[6-methylbenzo(4*H*-1,3,2)-dioxastannine] (**6**), and 2,2′-spirobi[6-methoxybenzo(4*H*-1,3,2)dioxastannine] (**7**). ^{13}C and ^{119}Sn NMR spectroscopy in the solid state and in solution as well as IR spectroscopy and elemental analysis were used to characterize the tin alkoxides. The molecular structures of compounds **2** and **3** were determined by single-crystal X-ray diffraction analysis. The moisture sensitivity of the tin(IV) alkoxides was demonstrated by the formation of the tin oxocluster $[Sn_3(\mu_3\text{-}O)(\mu_2\text{-}OH)(\mu_2\text{-}OCH_2C_4H_3S)_3(OCH_2C_4H_3S)_6(HOCH_2C_4H_3S)]_2$ (**2a**), a hydrolysis product of compound **2**. Polymerization reactions in the melt (for **1** and **5**) and in solution (for **2**–**4**) resulted in cross-linked nanocomposites of the type polymer/SnO_2. Subsequent oxidation of the composites gave SnO_2 with BET surface areas up to 178 m^2g^{-1}. Simultaneous twin polymerization of compounds **5**–**7** with the silicon derivative 2,2′-spirobi[4*H*-1,3,2-benzodioxasiline] resulted in the formation of polymer/SnO_2/SiO_2 hybrid materials. Oxidation gave porous materials with SnO_2 nanoparticles embedded in a silica network with BET surface areas up to 378 m^2g^{-1}. The silica acts as a crystal growth inhibitor, which prevents sintering of the SnO_2 nanoparticles 20–32 nm in size.

Introduction

There is an ongoing interest in the development of synthetic strategies for tin oxide, which results from its use in various technical applications. Well known is its utilization in gas sensors,[1–8] solar cells,[9–11] transparent electrodes,[9] heat-reflecting filters,[12] catalysts (e.g., CO oxidation),[13] and as anode materials for lithium-ion batteries.[14–21] Therefore, a variety of methods for the preparation of high-surface-area tin oxide have been reported, for example, sol–gel synthesis,[22–27] precipitation methods,[28,29] hydrothermal routes,[30,31] aqueous syntheses,[32–36] molten salt processes,[37] and methods using ultrasonic spraying.[38] However, the synthesis of SnO_2 nanoparticles with high surface area and without contamination, such as chloride, sodium, potassium, or carbon, is still a challenge. Recently, nonaqueous solution routes for the preparation of metal oxide nanoparticles were shown to be valuable methods to control the shape, size, and crystallinity of metal oxides.[39–42] Herein, we report a novel nonaqueous route to synthesize high-surface-area tin oxide nanoparticles using so-called twin polymerization (TP). This novel strategy was developed by Spange et al. for the synthesis of high-surface-area metal oxides, such as SiO_2[43,44] and TiO_2,[45] as well as for the preparation of metal oxide nanoparticles.[46] The concept of this synthetic route is the reaction of a well-defined metal-containing monomer to result in interpenetrating networks of, for example, a metal oxide and a polymer. Insight into some characteristic details was provided recently, which demonstrated the balance between the fast formation of a dense organic network that im-

[a] *C. Leonhardt, S. Brumm, Prof. Dr. M. Mehring*
Technische Universität Chemnitz
Fakultät für Naturwissenschaften
Institut für Chemie, Professur Koordinationschemie
Strasse der Nationen 62, 09111 Chemnitz (Germany)
Fax: (+49) (0)-371-531-21219
E-mail: michael.mehring@chemie.tu-chemnitz.de

[b] *Dr. A. Seifert*
Technische Universität Chemnitz
Fakultät für Naturwissenschaften
Institut für Chemie, Professur Polymerchemie
Strasse der Nationen 62, 09111 Chemnitz (Germany)

[c] *Dr. G. Cox, Dr. A. Lange*
BASF SE
Carl-Bosch Strasse 38, 67056 Ludwigshafen (Germany)

[d] *Dr. T. Rüffer, D. Schaarschmidt, Prof. Dr. H. Lang*
Technische Universität Chemnitz
Fakultät für Naturwissenschaften
Institut für Chemie, Professur Anorganische Chemie
Strasse der Nationen 62, 09111 Chemnitz (Germany)

[e] *N. Jöhrmann, M. Hietschold*
Technische Universität Chemnitz
Fakultät für Naturwissenschaften
Institut für Physik, Professur Analytik an Festkörperoberflächen
Reichenhainer Strasse 70, 09126 Chemnitz (Germany)

[f] *Dr. F. Simon*
Leibniz-Institut für Polymerforschung Dresden e.V.
Hohe Strasse 6, 01069 Dresden (Germany)

Supporting information for this article is available on the WWW under http://dx.doi.org/10.1002/cplu.201200242.

pedes phase separation and the slower formation of the inorganic network.[47] Most remarkably, the as-prepared organic–inorganic hybrid materials finally consist of two interpenetrating networks with domains in the nanometer range. In a subsequent oxidation step the carbon-containing material is removed and a metal oxide with high surface area is produced. The approach was recently extended to the concept of simultaneous twin polymerization (STP), which is classified as a process in which two well-defined precursors are polymerized simultaneously in a single process step to provide a single organic homopolymer and nanoscaled metal oxide phases.[48] Herein, both concepts, TP and STP, are applied for the first time to tin alkoxides to provide porous SnO_2 and SnO_2/SiO_2 composites.

Results and Discussion

The concept of TP is based on the preparation of well-defined tin-containing twin monomers that readily polymerize after addition of an initiator or upon heat treatment. All the tin compounds reported herein were prepared by transesterification of tetra-*tert*-butoxystannane or tetra-*tert*-pentyloxystannane with furfuryl alcohol, 2-thiophenemethanol, (2-methoxyphenyl)methanol, (2,4-dimethoxyphenyl)methanol, 2-(hydroxymethyl)phenol, 2-(hydroxymethyl)-4-methylphenol, and 2-(hydroxymethyl)-4-methoxyphenol to give compounds **1**–**7**, respectively (Scheme 1).

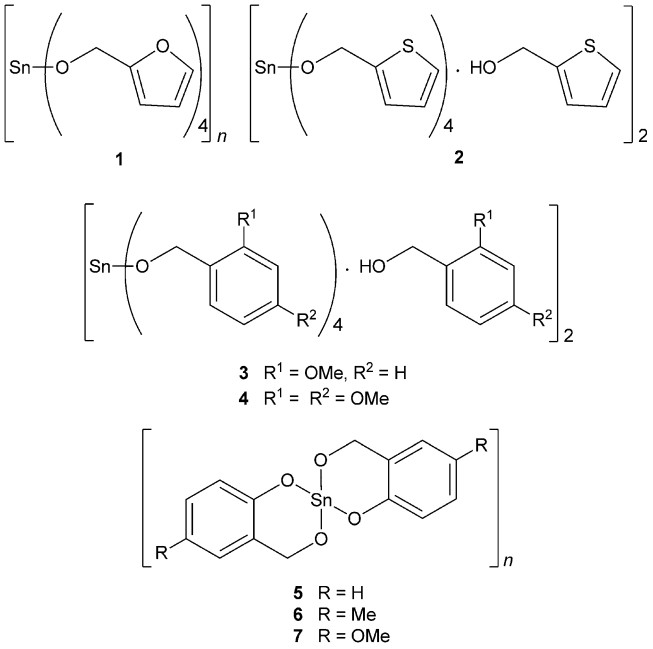

Scheme 1. Novel tin-containing precursors for twin polymerization.

The polymerization of the tin-containing precursors **1**–**7** results in polymer/SnO_2 hybrid materials that were subsequently oxidized to give porous SnO_2. Although this is in principle a nonaqueous synthetic route, the polymerization of the organic moiety in compounds **1**–**4** produces water as a byproduct. With regard to the moisture sensitivity of tin(IV) alkoxides, we additionally synthesized the novel tin-containing precursors **5**–**7**, which are based on "spirocyclic" structures. Such twin monomers do not eliminate water during the polymerization step, as was shown previously in the TP of the spirocyclic silicon compound 2,2′-spirobi[4*H*-1,3,2-benzodioxasiline] (Scheme 2).[44] The latter is also suitable as a precursor for the STP, in which the silicon derivative reacts simultaneously with a spirocyclic tin derivative of type **5**–**7** and hence serves as a template for the formation of nanosized SnO_2 in a SiO_2 matrix (see the section Simultaneous Twin Polymerization).

Synthesis and characterization of the tin monomers 1–7

Tetra(furan-2-ylmethoxy)stannane (**1**) is a highly moisture sensitive solid of low solubility, but a freshly prepared sample does not show IR bands for OH groups that are typically observed after partial hydrolysis. The analytical data for **1** support the suggested composition and the solid-state ^{13}C NMR spectrum shows the expected signals assigned to the furan-2-ylmethanolate ligand. Two different chemical environments for the tin atoms are suggested on the basis of two ^{119}Sn NMR chemical shifts of similar intensity at $\delta = -595$ and -602 ppm and the characteristic resonances at $\delta = 154$ and 159 ppm in the solid-state ^{13}C NMR spectrum (Figure 1).

Compared with compound **1** the moisture sensitivity of $[Sn(OCH_2C_4H_3S)_4{\cdot}HOCH_2C_4H_3S]_2$ (**2**) is reduced and its solubility

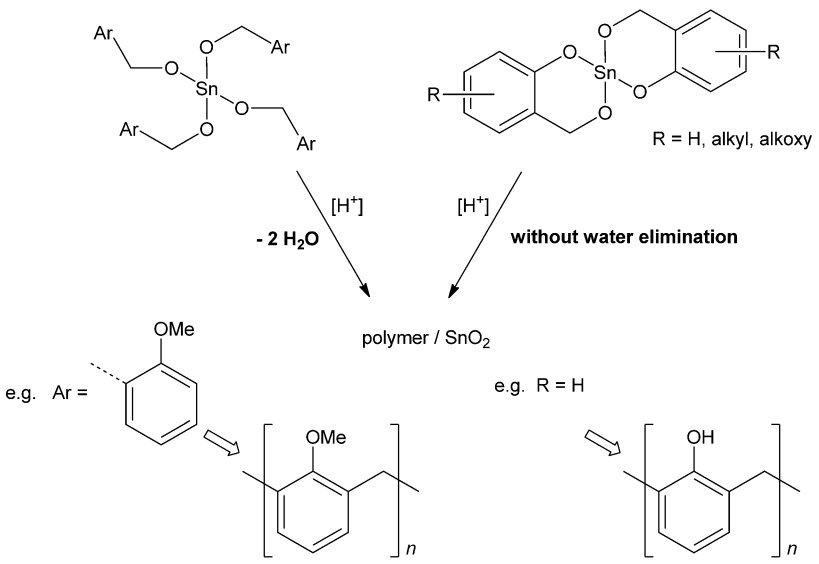

Scheme 2. Twin polymerization of tin(IV) alkoxides with and without elimination of water.

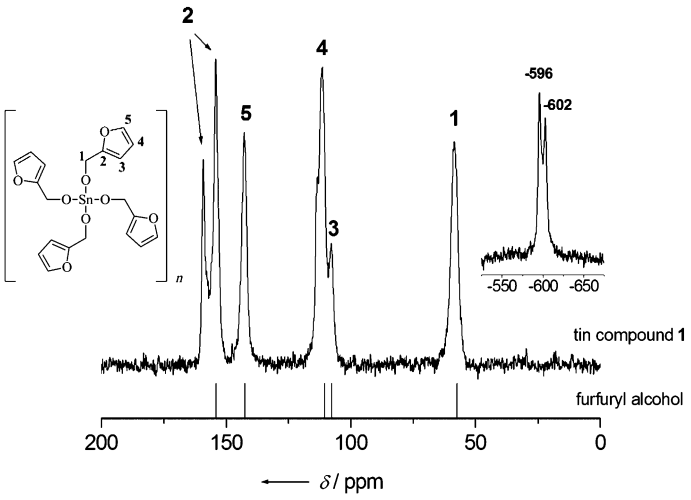

Figure 1. Solid-state ^{13}C-{^{1}H} cross-polarization magic angle spinning (CP-MAS) NMR spectrum of compound **1** compared with ^{13}C NMR data of furfuryl alcohol in $CDCl_3$. Inset: ^{119}Sn-{^{1}H}-MAS NMR spectrum of compound **1**.

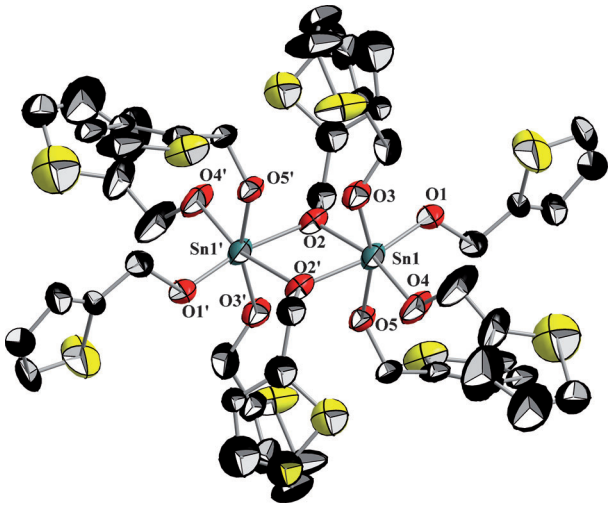

Figure 2. Molecular structure of $[Sn(OCH_2C_4H_3S)_4{\cdot}HOCH_2C_4H_3S]_2$ (**2**) as determined by single-crystal X-ray diffraction analysis. Thermal ellipsoid representation is at 50% probability level. Hydrogen atoms have been removed for clarity. Selected bond lengths [Å]: Sn1–O1 1.960(7), Sn1–O2 2.080(5), Sn1–O2′ 2.089(5), Sn1–O3 2.075(5), Sn1–O4 1.967(6), Sn1–O5 2.167(5); selected angles [°]: O1-Sn1-O2′ 91.8(3), O1-Sn1-O2 166.2(3), O1-Sn1-O4 101.0(3), O2′-Sn1-O2 74.4(2), O2′-Sn1-O4 164.2(3), O2-Sn1-O4 92.8(3), O3-Sn1-O1 95.3(3), O3-Sn1-O2′ 86.2(2), O3-Sn1-O2 82.4(2), O3-Sn1-O4 101.5(3), O3-Sn1-O5 161.8(2), O5-Sn1-O1 96.4(3), O5-Sn1-O2′ 79.5(2), O5-Sn1-O2 83.0(2), O5-Sn1-O4 90.0(2). The hydrogen atom of the coordinated alcohol was located at O5 (O5–H5 0.961(1) Å).

is enhanced. The molecular structure of compound **2** is shown in Figure 2 and selected bond lengths and angles are given in the caption. Compound **2** crystallizes in the triclinic space group $P\bar{1}$ with one formula unit per unit cell (see Table 1). The tin(IV) alkoxide **2** is isostructural with previously reported $[Sn(O\mathit{i}Pr)_4{\cdot}HO\mathit{i}Pr]_2$ and $[Sn(O\mathit{i}Bu)_4{\cdot}HO\mathit{i}Bu]_2$[49] as well as with $[Sn(OCH_2\text{-}2\text{-}OCH_3C_6H_4)_4{\cdot}HOCH_2\text{-}2\text{-}OCH_3C_6H_4]_2$ (**3**), which is also reported here (Figure S1 in the Supporting Information). Compounds of the general type $[Sn(OR)_4{\cdot}HOR]_2$ are built up by two edge-sharing octahedra with hexacoordinated tin atoms showing comparable tin–oxygen bond lengths. In compound **2** these amount to 1.960(7) Å for Sn(1)–O(1) and 1.967(6) Å for Sn(1)–O(4), which are both assigned to the two monodentate terminal ligands. The Sn–O bond lengths of the μ_2-oxygen ligands amount to 2.089(5) and 2.080(5) Å for Sn(1)–O(2) and Sn(1)–O(2′), respectively, and thus are comparable to the bond lengths Sn(1)–O(3) (2.075(5) Å) and Sn(1)–O(5) (2.167(5) Å) assigned to the two remaining terminal ligands. The latter two ligands form hydrogen bonds (O(3)–O(5) 2.639(3) Å) resulting in Sn–O bond elongation and distortion of the *trans* O(3)–Sn(1)–O(5) bond angle to 161.8(2)°. Despite the presence of methoxy groups attached to the benzylic ligand, which might coordinate intramolecularly, in compound **3** no such intramolecular coordination is observed. Thus, the molecular structure of compound **3** matches well that of compound **2**.

The ^{119}Sn NMR spectra in C_6D_6 of compounds **2**–**4** show single

Table 1. Crystallographic data for compounds **2**, **2a**, and **3**.

	2	**2a**·0.5 C_7H_8	**3**
empirical formula	$C_{50}H_{52}O_{10}S_{10}Sn_2$	$C_{100}H_{104}O_{24}S_{20}Sn_6{\cdot}0.5\,C_7H_8$	$C_{80}H_{92}O_{20}Sn_2$
formula weight [g mol^{-1}]	1371.01	3089.51	1610.99
crystal system	triclinic	triclinic	triclinic
crystal size [mm^3]	0.3×0.24×0.08	0.4×0.4×0.2	0.3×0.3×0.2
space group	$P\bar{1}$	$P\bar{1}$	$P\bar{1}$
unit cell dimensions			
a [Å]	10.4932(10)	14.1212(6)	12.0282(11)
b [Å]	11.624(1)	14.1373(6)	12.4422(9)
c [Å]	13.0284(13)	17.0598(8)	14.3736(17)
α [°]	71.263(8)	94.417(4)	67.219(9)
β [°]	79.290(8)	97.524(4)	68.641(9)
γ [°]	67.676(8)	115.899(4)	82.435(7)
Z	1	1	1
ρ_{calcd} [mg m^{-3}]	1.640	1.710	1.448
μ [mm^{-1}]	11.126	13.578	5.984
$F(000)$	692	1541	832
θ range for data collection [°]	4.28–62.00	3.54–62.00	3.55–64.15
index ranges	$-12 \le h \le 9$	$-16 \le h \le 15$	$-13 \le h \le 14$
	$-13 \le k \le 12$	$-16 \le k \le 16$	$-13 \le k \le 14$
	$-14 \le l \le 14$	$-19 \le l \le 19$	$-16 \le l \le 16$
reflections collected	9672	21 880	10 278
independent reflections/R_{int}	4310/0.0244	9122/0.0257	5988/0.0562
$R1$ (F) [$I > 2\sigma(I)$]	0.0671	0.0443	0.0522
$wR2$ (F^2) (all data)	0.1918	0.1356	0.1216
goodness-of-fit on F^2	1.082	1.121	0.889
largest diff. peak and hole [e Å^{-3}]	2.890/−1.418	1.733/−0.935	1.338/−0.827

resonances at $\delta = -623$, -622, and -623 ppm, respectively, thus confirming hexacoordination of the tin atoms for all three compounds in solution, as is demonstrated for compounds **2** and **3** in the solid state by single-crystal X-ray diffraction. Compound **4** shows a single ^{119}Sn NMR resonance at $\delta = -625$ ppm in the solid state, similar to its ^{119}Sn NMR resonance in solution. Hence, it is concluded that compound **4** adopts a structure in the solid state similar to that reported here for compounds **2** and **3**.

The moisture sensitivity of the tin(IV) alkoxides is demonstrated by the isolation of single crystals from a pentane solution of compound **2** after contact with moisture, which proved to be a hydrolysis product with the formula $[Sn_3(\mu_3\text{-}O)(\mu\text{-}OH)(\mu\text{-}OR)_3(OR)_6(HOR)]_2$ (R = $CH_2C_4H_3S$; **2a**). The molecular structure of the hexanuclear cluster **2a** is shown in Figure 3 and the inner tin–oxygen core structure is given in Figure S2.

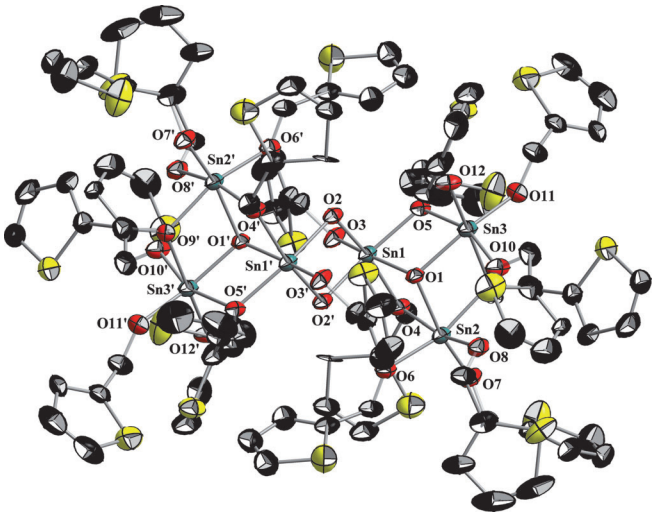

Figure 3. Molecular structure of $[Sn_3(\mu_3\text{-}O)(\mu_2\text{-}OH)(\mu_2\text{-}OCH_2C_4H_3S)_3(OCH_2C_4H_3S)_6(HOCH_2C_4H_3S)]_2 \cdot 0.5\,C_7H_8$ (**2a**·0.5 C_7H_8) as determined by single-crystal X-ray diffraction analysis. Thermal ellipsoid representation is at 50% probability level. Hydrogen atoms and disordered toluene molecules have been removed for clarity. Selected bond lengths and angles are given in the caption of Figure S2, which shows the tin–oxygen core structure.

The hexanuclear cluster might be regarded as a hydroxy-bridged dimer of $[Sn_3(\mu_3\text{-}O)(\mu\text{-}OH)(\mu\text{-}OR)_3(OR)_6(HOR)]$. This type of trinuclear structure was first reported by Reuter and Kremser for R = *i*Bu.[50] The hydrogen atoms were not located for **2a** but the long distances corresponding to Sn(1)–O(2) and Sn(1)–O(2′) (2.089(4) and 2.098(4) Å) in combination with the distance O(2)–O(6′) of 2.732(6) Å, which is in the range typically observed for weakly hydrogen bonded systems, confirm the OH assignment. The presence of the coordinated alcohol ROH at O(10) is deduced from the presence of a quite short oxygen–oxygen distance O(10)–O(8) of 2.466(6) Å, which is indicative of a strong hydrogen bond, and the elongated tin–oxygen distance Sn(3)–O(10) of 2.130(4) Å, as compared with Sn(2)–O(8) of 2.053(4) Å.

2,2′-Spirobi[4*H*-1,3,2-benzodioxastannine] (**5**) is a moisture-sensitive solid material with low solubility in common organic solvents that decomposes at 250 °C. The suggested composition is supported by elemental analysis and IR and NMR spectroscopy. The solid-state ^{13}C NMR spectrum of compound **5** shows the expected signals assigned to the 2-(oxidomethyl)-phenolate ligand (Figure 4). The signal assigned to the methylene group is shifted downfield from $\delta = 64$ ppm (salicyl alcohol) to $\delta = 71$ ppm in compound **5**. The ^{119}Sn NMR chemical shift in the solid state at $\delta = -697$ ppm confirms hexacoordination of the tin atom and excludes the formation of mononuclear species.[51–53]

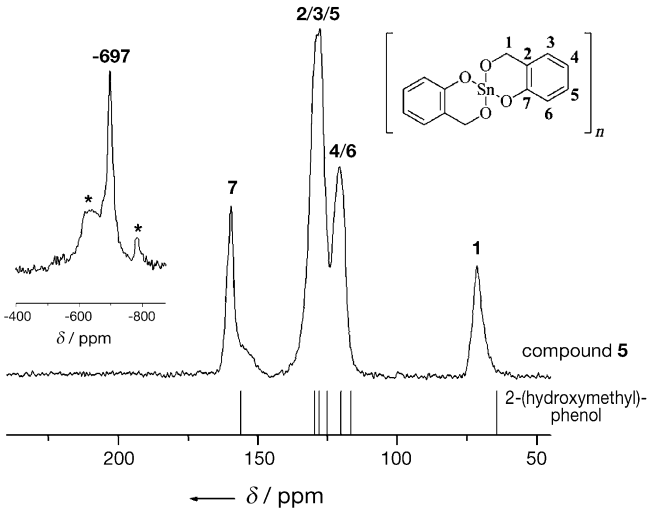

Figure 4. Solid-state ^{13}C-{^{1}H}-CP-MAS NMR and ^{119}Sn-{^{1}H}-MAS NMR spectra (inset) of compound **5** and comparison with ^{13}C NMR data of 2-(hydroxymethyl)phenol in $CDCl_3$. Asterisks (*) indicate spinning side bands.

This assumption is also reinforced by comparison of the solid-state ^{119}Sn NMR data of the tetracoordinated tin atom in $Sn(OtBu)_4$ ($\delta = -371$ ppm) with the hexacoordinated tin atom in $[Sn(OiPr)_4 \cdot HOiPr]_2$ ($\delta = -648$ ppm).[49] The significant high-field shift is thus a result of the increase of the coordination sphere of the tin atom from four in mononuclear $Sn(OtBu)_4$ to six in the coordination polymer 2,2′-spirobi[4*H*-1,3,2-benzodioxastannine] (**5**). Introduction of a CH_3 or OCH_3 substituent at the 6-position to give 2,2′-spirobi[6-methylbenzo(4*H*-1,3,2)dioxastannine] (**6**) and 2,2′-spirobi[6-methoxybenzo(4*H*-1,3,2)dioxastannine] (**7**) significantly enhances the solubility of the precursors in common organic solvents compared with compound **5**. Similar to the tin alkoxide **5**, the IR spectra of compounds **6** and **7** do not show OH absorption bands and the CHN analyses confirm the suggested compositions. The solid-state ^{119}Sn NMR spectra reveal signals at $\delta = -705$ and -683 ppm for compounds **6** and **7**, respectively, which indicates hexacoordination of the tin atom and formation of coordination polymers in the solid state similar to compound **5**.[51–53] The solid-state ^{13}C NMR spectra of the tin precursors **6** and **7** (Figure S3) are quite similar to that of compound **5**, besides additional signals at $\delta = 20$ and 55 ppm for the CH_3 and OCH_3 groups, respectively.

Twin polymerization

To explore whether the novel tin monomers are suitable precursors for the so-called twin polymerization (TP), compounds **1** and **5** were converted in the melt and compounds **2**–**4** in $CHCl_3$ solution into organic–inorganic hybrid materials of the type **A**–**E** (Scheme 3).

In solution, addition of an initiator such as CF_3SO_3H to $CHCl_3$ solutions of compounds **2**–**4** is necessary to give a spontaneous reaction, whereas polymerization of the tin precursor **1** in the melt is self-initiated by its Lewis acidic nature to give hybrid material **A**. The thermally induced polymerization of compound **5** requires the use of acids, such as 4-methylbenzenesulfonic acid, as initiator to produce hybrid material **E**, otherwise decomposition to give undefined components is observed. CF_3CO_2H-induced polymerization of compounds **2** and **3** proceeds sluggishly and low conversion to give the hybrid materials **B**′ and **C**′ is observed (Table 2).

Table 2. Conditions for polymerization reactions of the tin precursors **1**–**5**.

Compound	Solvent	Initiator	M/I[a]	Hybrid material, reaction time	Carbon content [%] found[b]/calcd[c]
1	melt	–	–	**A**, 3 h	20.5/51.0
2	$CHCl_3$	CF_3SO_3H	1:0.02	**B**, spontaneous reaction	41.5/47.6
2	$CHCl_3$	CF_3CO_2H	1:0.05	**B**′, 3 months	33.1/47.6
3	$CHCl_3$	CF_3SO_3H	1:0.05	**C**, spontaneous reaction	23.5/63.9
3	$CHCl_3$	CF_3CO_2H	1:0.1	**C**′, 36 h	19.2/63.9
4	$CHCl_3$	CF_3SO_3H	1:0.05	**D**, spontaneous reaction	50.8/59.9
5	solid	4-$CH_3C_6H_4SO_3H$	1:0.1	**E**, 15 min	42.6/46.3

[a] Based on number of ligands per tin atom. M = monomer, I = initiator. [b] Carbon content of the nanocomposite material after workup. [c] Carbon content expected for quantitative conversion into polymer/SnO_2.

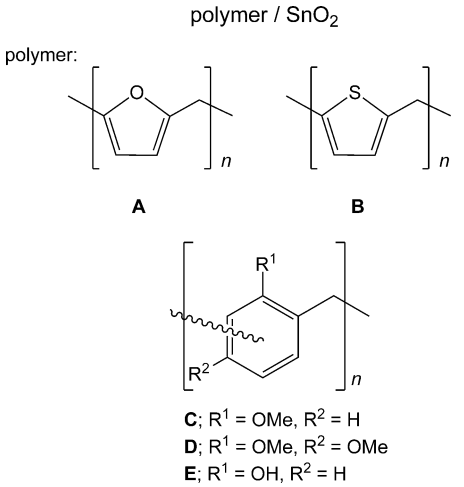

Scheme 3. Organic–inorganic hybrid materials **A**–**E** composed of SnO_2 embedded in a polymer matrix.

The hybrid materials were analyzed by CHN analyses and solid-state (^{13}C, ^{119}Sn) NMR spectroscopy. For example, the final black hybrid material **A**, obtained by thermally induced polymerization of compound **1**, contains a low carbon content of 20.5%, which is significantly lower than expected for quantitative conversion (calcd 51%). However, the absence of a signal for the $SnOCH_2$ group and the presence of a typical signal for a methylene group of poly(furfuryl alcohol) (PFA) in the solid-state ^{13}C NMR spectrum indicate polymerization of the tin precursor (Figure 5). The broad ^{119}Sn NMR signal, relative to crystalline SnO_2, results from the embedding of amorphous or nanocrystalline SnO_2[54] and most likely some incompletely condensed tin oxide precursors within the polymer matrix (Figure 6).

The low carbon content of the hybrid material **A** is explained by the formation of soluble oligomers that are removed by the workup procedure, which is confirmed by the ^{13}C-{^1H}-CP-MAS NMR spectrum of PFA/SnO_2 (**A**) that shows several signals of high intensity assigned to end groups of incompletely polymerized PFA (Figure 5).[45,55] In contrast to compound **1**, TP of compound **2** gave almost complete conversion into the poly(-thiophene-2-methanol)/SnO_2 hybrid material **B** (Table 2). The solid-state ^{13}C NMR spectrum is indicative of a high degree of polymerization and the solid-state ^{119}Sn NMR spectrum as well as electron diffraction are in accordance with the formation of SnO_2 entrapped in the polymer matrix (Figures 7 and S3). TEM analysis of **B** is indicative of the formation of crystalline SnO_2 primary particles 2–3 nm in size, consistent with powder X-ray diffraction (PXRD) studies (Table 3), which tend to some agglomeration in the polymer matrix.

Compounds **3** and **4** both react spontaneously in $CHCl_3$ upon addition of CF_3SO_3H to give a hybrid material, in the case of **3** (hybrid material **C**) with a low (C_{found} = 23.5%; C_{calcd} = 63.9%) and in the case of **4** (hybrid material **D**) with a high extent (C_{found} = 50.8%; C_{calcd} = 59.9%) of conversion. The ^{13}C and ^{119}Sn NMR spectra of hybrid material **C** are indicative of the formation of SnO_2 within the polymer matrix, similar to

Table 3. Parameters for the oxidation of hybrid materials **A**–**E** and BET surface area, crystallite size, and carbon content of the as-prepared SnO_2.

Hybrid material	Oxidation T [°C]/t [h]	BET surface area [m^2g^{-1}]	Crystallite size of SnO_2[c] [nm]	Carbon content in the oxidized material [%]
A	500/10[a]	87	8	–
A	600/10[a]	57	14	–
A	700/10[a]	42	32	–
A	800/10[a]	34	36	–
A	900/10[a]	–[d]	45	–
B′	600/10[b]	178	4	0.50
C	600/5[b]	133	9	0.28
C′	450/5[b]	137	12	–
D	600/5[b]	78	9	0.38
E	600/1	143	6	–

[a] Heating rate 2 $K\,min^{-1}$. [b] Heating rate 5 $K\,min^{-1}$. [c] Calculated using the Scherrer equation. [d] Not measured.

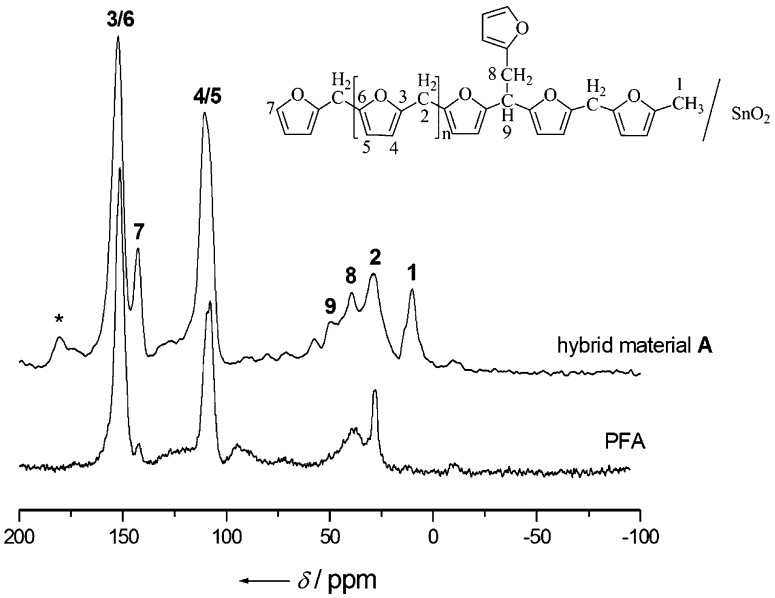

Figure 5. Solid-state ^{13}C-{^{1}H}-CP-MAS NMR spectra of PFA/SnO_2 (**A**) and pure PFA. The asterisk (*) indicates a spinning side band.

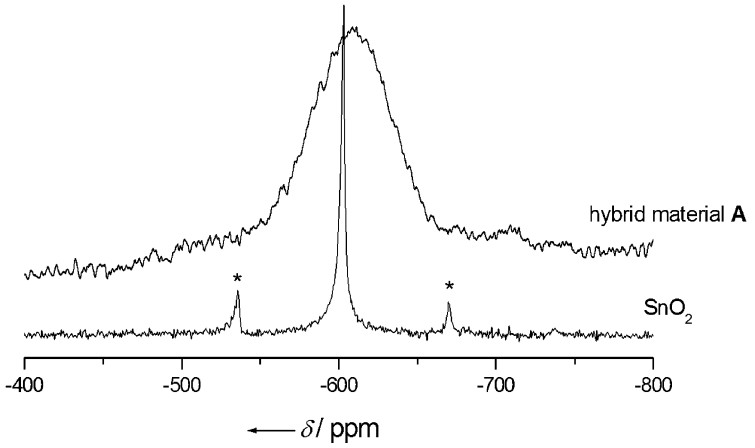

Figure 6. Solid-state ^{119}Sn-{^{1}H}-MAS NMR spectra of PFA/SnO_2 (**A**) and crystalline SnO_2. Asterisks (*) indicate spinning side bands.

compound **1** (Figure S4). However, the degree of polymerization is low and oligomers are removed upon workup.

In the case of compound **4**, almost complete conversion to give calix[4]resorcinarene octamethyl ether/SnO_2 as a result of cyclooligomerization instead of polymerization is observed. The half-height width of the ^{119}Sn NMR signal is reduced to $\nu_{1/2} = 2685$ Hz for the hybrid material **D** as compared to $\nu_{1/2} = 8344$ Hz in the hybrid material **C** (Figure S5). We were able to separate and crystallize the calix[4]resorcinarene octamethyl ether by sublimation. Information about its single-crystal X-ray structure analysis, including its molecular structure, is given in Table S1 and Figure S6.

HAADF-STEM analysis of the hybrid material **C** indicates that tin(IV)oxide nanoparticles (≈2–4 nm) are formed, which build agglomerates (Figure S7). Similarly, hybrid material **D** consists of SnO_2 agglomerates on the micrometer scale with primary particle size of 2–4 nm and shows an inhomogeneous distribution of SnO_2 particles in the polymer matrix.

The thermally induced polymerization of **5** results in almost quantitative conversion indicated by a carbon content of 42.6% (calcd 46.3%) for the hybrid material **E**. The broad signal at $\delta = 33$ ppm in the ^{13}C NMR spectrum is characteristic for the formation of methylene groups in a phenolic resin. In addition to *ortho–ortho'* there is also *ortho–para'* linkage between the monomeric units in the polymer, as indicated by a signal at $\delta = 116$ ppm (the *ortho* and *para* assignments are relative to the hydroxyl-substituted carbon).[56–58] As observed for the hybrid material **A**, the broad signal at $\delta = -607$ ppm ($\nu_{1/2} = 9996$ Hz) in the solid-state ^{119}Sn NMR spectrum indicates the formation of nanocrystalline SnO_2 and/or an incompletely condensed tin oxide-based material (Figure S8).[54]

Oxidation of the hybrid materials

Thermogravimetric analyses of the hybrid materials **A**–**E** were performed to compare the thermal behavior with that of the pure polymers and calix[4]resorcinarene octamethyl ether, respectively, and to identify the ideal decomposition temperature to remove carbon (Figure S9). For all hybrid materials decomposition under air to give crystalline SnO_2 is completed below 600 °C. Thus, in the case of the hybrid materials **A**–**C** and **E**, the full decomposition is observed at a lower temperature than for the oxidation of the pure polymers. In the case of hybrid material **D**, decomposition of calix[4]resorcinarene octamethyl ether is not altered significantly by the presence of SnO_2.

Additionally, the thermal behavior of reference samples was studied to analyze whether the addition of SnO_2 nanoparticles to a separately prepared polymer matrix significantly influences the decomposition temperature (Figure S10). For example, the thermal behavior of a sample prepared by mechanically mixing SnO_2 nanoparticles (29 nm) with poly(2-methoxybenzyl alcohol) is comparable to that of the pure polymer and the decomposition is completed at 720 °C. In contrast, the thermal

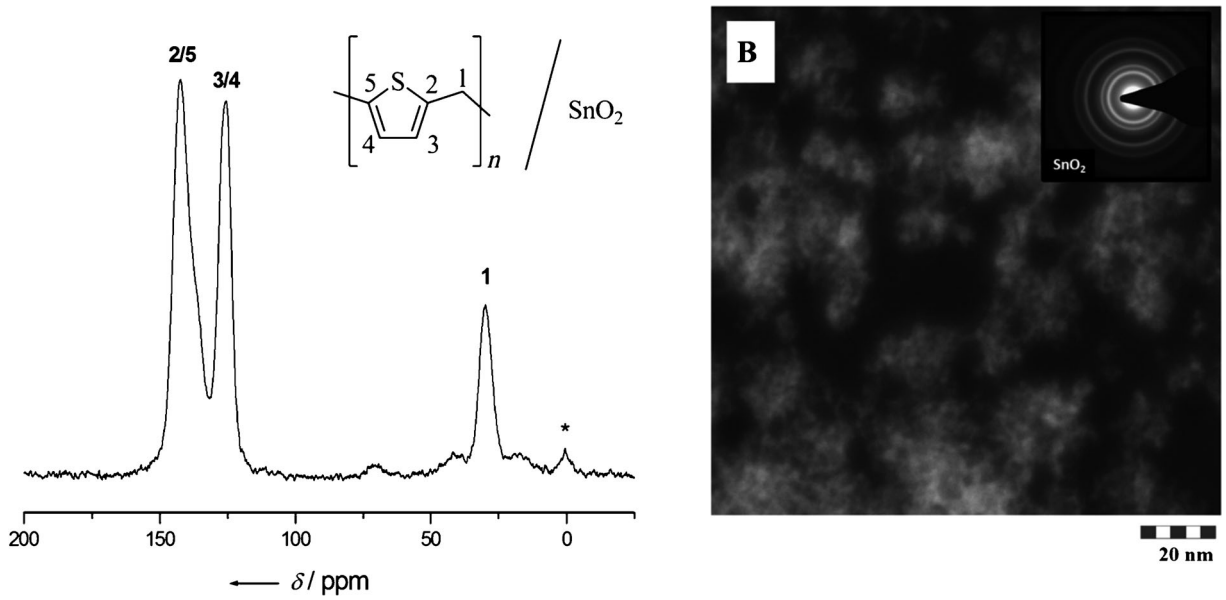

Figure 7. Left: Solid-state ^{13}C-{^{1}H}-CP-MAS NMR spectrum of poly(thiophene-2-methanol)/SnO_2 hybrid material **B** (CF_3SO_3H-initiated). The asterisk (*) indicates a spinning side band. Right: High-angle annular dark-field (HAADF)–scanning electron transmission microscopy (STEM) image of poly(thiophene-2-methanol)/SnO_2 hybrid material **B** (CF_3SO_3H-initiated). Inset: Selected-area electron diffraction of hybrid material **B**.

behavior of a hybrid material prepared by polymerization of (2-methoxyphenyl)methanol in the presence of SnO_2 nanoparticles (29 nm) is different. Complete decomposition of the polymeric resin is observed at 600 °C, only slightly above the temperature for the complete decomposition of the organic parts in the corresponding hybrid material **C**.

Based on these results we have chosen oxidation temperatures for the bulk materials **B**–**E** of 450 to 600 °C. For comparison, oxidation of the hybrid material PFA/SnO_2 (**A**) was performed between 500 and 900 °C in steps of 100 °C. Notably, SnO_2 prepared from **A** did not show the presence of residual carbon. As expected the primary particle size, as calculated from PXRD patterns, is increased from 8 to 45 nm by increasing the oxidation temperature stepwise to 900 °C and the BET surface area is reduced (Table 3, Figure 8).

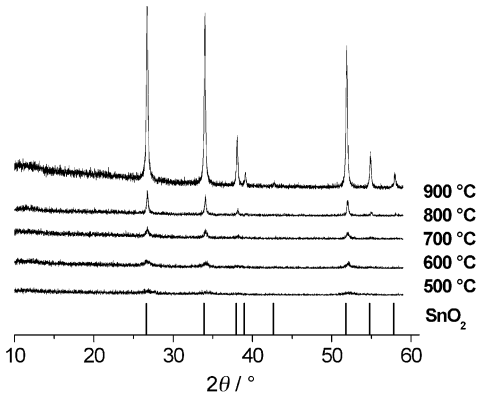

Figure 8. PXRD pattern from hybrid material **A** oxidized with air in a temperature range of 500–900 °C (heating rate: 2 K min^{-1}, oxidation time 10 h). SnO_2: JCPDS 01-070-4175.

The highest BET surface area of 178 m^2 g^{-1} was observed for the final material obtained upon oxidation of the hybrid material **B**′. The residual carbon content of 0.50 % is quite low. Starting from hybrid material **C**, BET surface areas of 133 m^2 g^{-1} (residual carbon content: 0.28 %) and 137 m^2 g^{-1} (no residual carbon detected) were observed, which is in the same range as that observed for the final material obtained by oxidation of hybrid material **E** (143 m^2 g^{-1}, no residual carbon content). The oxidized hybrid material **D** (78 m^2 g^{-1}, residual carbon content: 0.38 %) shows a smaller BET surface area than the final materials obtained from **B**′, **C**, and **E** and is in the same range as for the oxidized materials starting from hybrid material **A**. TEM images of the calcined materials $\mathbf{A}_{ox}$(500 °C), $\mathbf{B}'_{ox}$(600 °C), and $\mathbf{C}'_{ox}$(450 °C) (Figure 9) show that the particle size is consistent with PXRD in the range 5–15 nm and that the materials $\mathbf{A}_{ox}$ and $\mathbf{C}'_{ox}$ do not differ significantly. Somewhat smaller particles 5–10 nm in size are obtained for material $\mathbf{B}'_{ox}$.

Simultaneous twin polymerization

To prepare SnO_2/SiO_2 composites we chose the concept of simultaneous twin polymerization (STP). Thus, starting from mixtures of the silicon monomer 2,2′-spirobi[4*H*-1,3,2-benzodioxasiline] (Si-spiro, m.p. 82–84 °C) and the tin alkoxides **5**–**7** in a 2:1 ratio, organic–inorganic hybrid materials are observed, which are transformed into SnO_2/SiO_2 composites by subsequent oxidation (Scheme 4). In the first step homogeneous melts were observed and heated at temperatures of 80–100 °C for 30 min to give a solid material. After the workup procedure to remove soluble components, high carbon contents of the organic–inorganic hybrid materials are indicative of effective cross-linking of the polymer (Table 4). Notably, addition of an

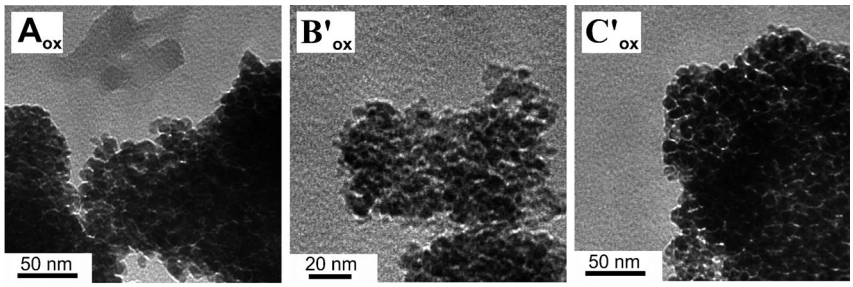

Figure 9. TEM images of the oxidized hybrid materials $\mathbf{A}_{ox}$(500 °C), $\mathbf{B'}_{ox}$(600 °C), and $\mathbf{C'}_{ox}$(450 °C).

Table 4. Simultaneous twin polymerization of 2,2′-spirobi[4*H*-1,3,2-benzodioxasiline] with the tin alkoxides **5**–**7**.

Tin precursor[a]	Polymerization in melt T [°C]/t [h]	Carbon content [%] found[b]/calcd[c]	Hybrid material
5	100/0.5	48.5/55.6	**F**
6	100/0.5	51.5/56.5	**G**
7	80/0.5	48.7/54.6	**H**

[a] Si/Sn ratio 2:1. [b] Carbon content of the nanocomposite material after workup. [c] Carbon content expected for quantitative conversion into polymer/SnO_2/SiO_2 hybrid materials.

initiator is not necessary, because the reaction is self-initiated by the Lewis acidic nature of the tin alkoxides.

Solid-state ^{13}C NMR spectra of the hybrid materials **F**–**H** (Figure 10) show a high-field shift for the $SiOCH_2$ and $SnOCH_2$ groups to 31 ppm compared with the parent alcohol, which is characteristic for methylene bridges in polymeric structures. *Ortho–ortho′* and *ortho–para′* linkage in the polymer domains is deduced from signals at $\delta = 121$ and 116 ppm, respectively. In contrast to **H**, the hybrid materials **F** and **G** show ^{13}C NMR signals of weak intensity in the range $\delta = 60$–72 ppm and at $\delta = 158$ ppm that are indicative of unreacted Sn/Si–O–CH_2Ar moieties. This observation is in accordance with the expected high reactivity of the methoxy-substituted tin alkoxide **7**. Hybrid materials **F** and **G** show quite sharp signals in the solid-state ^{119}Sn NMR spectra at $\delta = -696$ and -706 ppm, respectively, whereas the hybrid material **H** shows a rather broad signal in the range $\delta = -600$ to -700 ppm. In the solid-state ^{29}Si NMR spectra signals at $\delta = -94$ and -101 ppm (for **F**), $\delta = -94$ ppm (for **G**), and $\delta = -98$ ppm (for **H**) are observed (Figure S11). The formation of stannosilicates is thus ruled out, as they typically show ^{29}Si NMR chemical shifts in the range of $\delta = -78$ to -91 ppm.[51,59,60] The solid-state NMR data indicate that the less reactive compounds **5** and **6** are not fully converted into SnO_2 as is observed for the more reactive compound **7**. The amorphous character of the hybrid materials **F**–**H** was shown by PXRD. Electron microscopy of the hybrid materials **F**–**H** shows the typical morphology of twin polymers[44,46,55] with organic and inorganic domains in the range of 20–40 nm and primary particles with a size of about 3 nm (Figure S12).

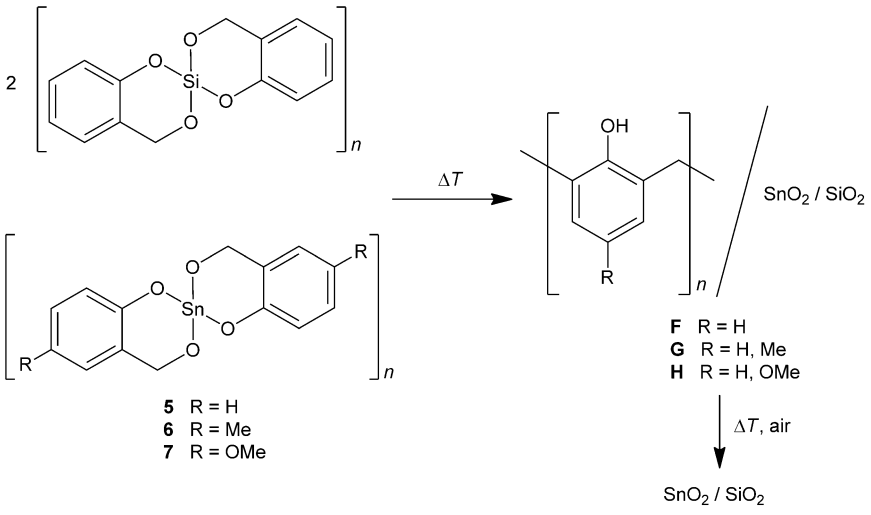

Scheme 4. Simultaneous twin polymerization of 2,2′-spirobi[4*H*-1,3,2-benzodioxasiline] and compounds **5**–**7** to give a hybrid material consisting of phenolic resins (e.g., *o*/*o′* substitution), SnO_2, and SiO_2.

Oxidation reactions

The as-prepared polymer/SnO_2/SiO_2 materials were oxidized in synthetic air to give porous SnO_2/SiO_2 hybrid materials. The optimum for the oxidation temperatures to remove the carbon was determined by thermogravimetric analyses (Table 5).

X-ray photoelectron spectroscopy measurements demonstrate that tin exclusively in the oxidation state IV is present. The Sn 3d element spectra show typical peak maxima of the Sn $3d_{5/2}$ peaks for SnO_2.[61] In addition, the calculated tin/silicon ratio was determined from the high-resolution Sn 3d and Si 2p element spectra, which amount to 0.23 (corresponds to 37 wt% SnO_2, for $\mathbf{F}_{ox}$), 0.27 (corresponds to 41 wt% SnO_2, for $\mathbf{G}_{ox}$), and 0.47 (corresponds to 54 wt% SnO_2, for $\mathbf{H}_{ox}$) (see Figure S13). Only $\mathbf{H}_{ox}$ shows the expected tin/silicon ratio assuming quantitative conversion of both precursors into the hybrid material. The less reactive tin species are not fully polymerized and thus are removed during the workup process. The detected peak maxima of the Si 2p peaks are in the upper range, as usually observed for SiO_2 and silicates.[62,63] Notably, in all materials the broad half-width of the Si 2p element spectra indicates a variation of bonding states of the silica-based material, thus demonstrating different electron densi-

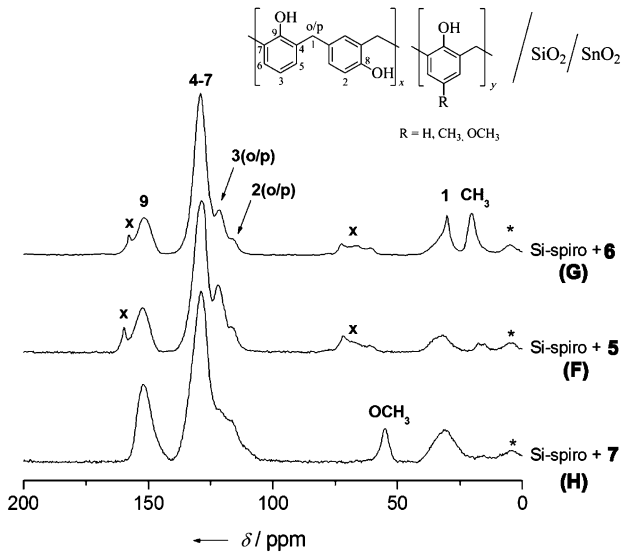

Figure 10. Solid-state ^{13}C-{^{1}H}-CP-MAS NMR spectra of hybrid materials **F**–**H**. Asterisks (*) indicate spinning side bands. The × indicates signals that are assigned to the unreacted tin compounds and/or incompletely condensed precursors.

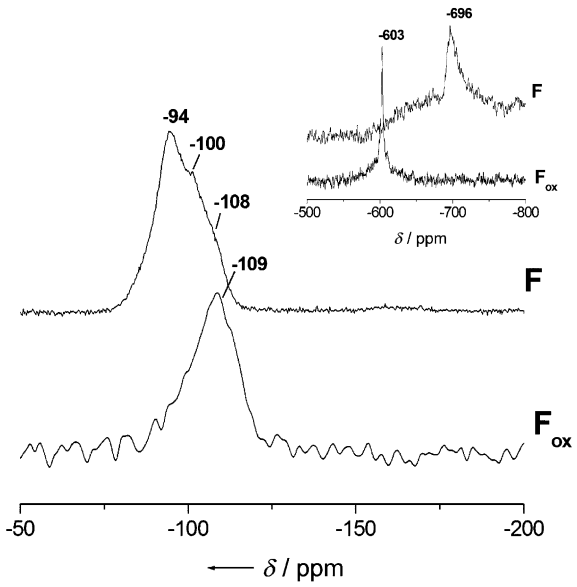

Figure 11. Solid-state ^{29}Si-{^{1}H}-CP-MAS NMR and ^{119}Sn-{^{1}H}-MAS NMR spectra (inset) of hybrid materials **F** and $\mathbf{F_{ox}}$.

Table 5. Analytical data for SnO_2/SiO_2 composites ($\mathbf{F_{ox}}$, $\mathbf{G_{ox}}$, and $\mathbf{H_{ox}}$) obtained by oxidation of the organic–inorganic hybrid materials **F**–**H**.

SnO_2/SiO_2 hybrid material	Oxidation[a] T [°C]/t [h]	BET surface area [$m^2 g^{-1}$]	Crystallite size of SnO_2[b] [nm]	Carbon content in the oxidized material [%]
$\mathbf{F_{ox}}$	800/5	227	25	0.02
$\mathbf{G_{ox}}$	700/5	165	32	0.03
$\mathbf{H_{ox}}$	700/5	378	20	0.09

[a] Heating rate 10 K min^{-1}. [b] Calculated using the Scherrer equation.

ties as result of hydrogen bonding, the presence of Si–OH groups, or the partial incorporation of tin. The solid-state ^{29}Si NMR spectrum of the hybrid materials such as **F** shows signals at $\delta = -94$ ppm (Q_2), $\delta = -100$ ppm (Q_3), and $\delta = -109$ ppm (Q_4) (Figure 11). The signals for $Q_{2/3}$ are indicative of an incompletely condensed silicon oxide phase (Si–OH or $Si(OH)_2$ moieties) and the Q_4 signal is typical for fully condensed SiO_2. The degree of condensation was increased by oxidation as is demonstrated by a shift of the ^{29}Si NMR signal to $\delta = -109$ ppm for the oxidized hybrid material $\mathbf{F_{ox}}$. In the corresponding ^{119}Sn NMR spectrum the signal is shifted from $\delta = -696$ ppm, as observed in the polymer-based hybrid **F**, to $\delta = -603$ ppm ($\nu_{1/2} = 2533$ Hz) for the oxidized material SiO_2/SnO_2 ($\mathbf{F_{ox}}$), which is indicative of amorphous or nanocrystalline SnO_2.[54]

The PXRD patterns of the SiO_2/SnO_2 hybrid materials are indicative of the formation of SnO_2 primary particles approximately 20 to 32 nm in size embedded in an amorphous SiO_2 matrix (Figure S14). The corresponding TEM images confirm that small particles are present with sizes in the range from 5 to 25 nm for $\mathbf{F_{ox}}$ and 5 to 32 nm for $\mathbf{G_{ox}}$ (Figure 12). Notably, a smaller crystallite size of the SnO_2 particles is obtained by STP of 2,2′-spirobi[4*H*-1,3,2-benzodioxasiline] with compounds **5**–**7** compared with TP of compounds **1**–**5**. Hence, the silica acts as a crystal growth inhibitor for SnO_2 during the oxidation process.

The BET surface areas of the SnO_2/SiO_2 materials range from 165 $m^2 g^{-1}$ for **F** to 378 $m^2 g^{-1}$ for **H** (Table 5). Nitrogen adsorption–desorption isotherms (Figure S15) of the as-prepared SnO_2/SiO_2 materials exhibit isotherm curves between type I and type IV. The isotherms of the oxidized hybrid materials $\mathbf{F_{ox}}$ and $\mathbf{G_{ox}}$ show hysteresis loops (type H4), which are characteristic for mesoporous solids, whereas the isotherm curve of $\mathbf{H_{ox}}$ shows a barely perceptible hysteresis loop and a steep rise, which is typical for microporous solids (type H1).[64,65] The pore size distribution as calculated by the DFT method reveals that the materials $\mathbf{F_{ox}}$ and $\mathbf{G_{ox}}$ are mainly mesoporous with pore sizes between 2 and 15 nm,

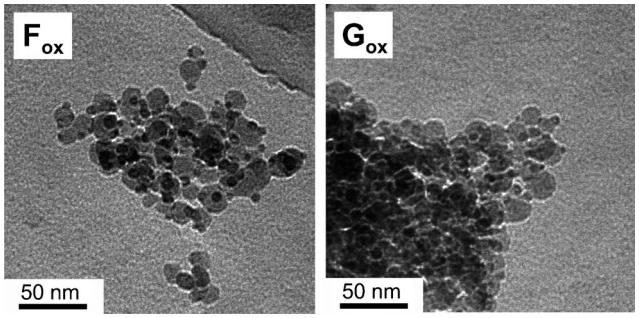

Figure 12. TEM images of the SnO_2/SiO_2 hybrid materials $\mathbf{F_{ox}}$ and $\mathbf{G_{ox}}$.

whereas in H_{ox} smaller pore sizes between 1 and 5 nm dominate.

As expected, the BET surface areas are significantly lower than that observed for mesoporous SiO_2 prepared by TP of 2,2′-spirobi[4*H*-1,3,2-benzodioxasiline] (904 $m^2 g^{-1}$),[44] but comparable with the highest values reported for SnO_2/SiO_2 hybrid materials prepared by the sol–gel process.[66] SiO_2/SnO_2 materials with tin oxide content of 22 and 29 wt% show surface areas in the range 269–343 $m^2 g^{-1}$ (heat treatment 700–400 °C)[23] and 375–494 $m^2 g^{-1}$ (heat treatment 800–400 °C),[67] whereas with increasing tin oxide content of 90 and 75 wt% surface areas of 211–340 $m^2 g^{-1}$ (heat treatment 600–400 °C)[31] and 133–209 $m^2 g^{-1}$ (heat treatment 800–400 °C)[30] have been reported. The SiO_2/SnO_2 materials obtained from the TP show comparatively high surface areas up to 378 $m^2 g^{-1}$ (700 °C heat treatment) with a tin oxide content of 54 wt%. Notably, long aging times for the preparation of xerogels, which in some cases are several days or even weeks, are not necessary in the TP process.[67,68]

Conclusion

Seven novel tin(IV) alkoxides **1**–**7** with potential for so-called twin polymerization were obtained by transesterification starting from $Sn(OR)_4$ (R = *t*Bu, *t*Am: 2-methyl-2-butyl) and furfuryl alcohol, 2-thiophenemethanol, (2-methoxyphenyl)methanol, (2,4-dimethoxyphenyl)methanol, 2-(hydroxymethyl)-4-methylphenol, and 2-(hydroxymethyl)-4-methoxyphenol, respectively. Compounds **2**–**4**, **6**, and **7** are soluble in organic solvents, whereas compounds **1** and **5** are not. Hence, polymerization reactions of **1** and **5** were performed without the use of a solvent, whereas the other precursors were reacted in solution to give polymer/SnO_2 hybrid materials. In the case of **4**, cyclooligomerization to give calix[4]resorcinarene octamethyl ether instead of a polymer is observed. Thus, it is concluded that the (2,4-dimethoxybenzyl)oxy substituent is not well suited as a ligand for twin polymerization, despite its high reactivity. In the case of polymerization of the tin precursors **2**–**5** in solution, CF_3SO_3H is the most effective initiator for the cationic polymerization. The use of CF_3COOH results in lower yields and longer reaction times. Starting from the hybrid materials obtained from compounds **1**–**5**, high-surface-area tin(IV)oxide with BET surface area up to 178 $m^2 g^{-1}$ is accessible by treatment of the hybrid materials with air at approximately 600 °C. Materials with higher surface area of up to 378 $m^2 g^{-1}$ composed of SnO_2/SiO_2 are accessible by using the concept of simultaneous twin polymerization in which 2,2′-spirobi[4*H*-1,3,2-benzodioxasiline] is reacted with tin precursors such as compounds **5**–**7** resulting in polymer/SnO_2/SiO_2 nanocomposites, which are finally oxidized to remove the organics. Notably, the polymerization is self-initiated as a result of the high Lewis acidity of the tin compounds and addition of any additional initiator even at temperatures below 100 °C is not necessary. In the as-prepared SnO_2/SiO_2 materials, the SiO_2 network inhibits the crystal growth of the simultaneously formed SnO_2 particles that exhibit crystallite sizes of approximately 20 nm. The extension of this concept to other metal oxide/SiO_2 composites is currently being investigated in our laboratories.

Experimental Section

General procedures and starting materials

All reactions were performed under inert argon atmosphere. Diethyl ether, *n*-pentane, and toluene were distilled over sodium before use. Tetra-*tert*-butoxystannane and tetra-*tert*-pentyloxystannane were prepared from $SnCl_4$ according to literature procedures.[49] Furfuryl alcohol was purchased from Merck KGaA and distilled over sodium hydride before use. 2-Thiophenemethanol and 2-methoxybenzyl alcohol were purchased from Alfa Aesar and used without further purification. 2,4-Dimethoxybenzyl alcohol was prepared from 2,4-dimethoxybenzaldehyde.[69] SnO_2 nanoparticles were purchased from Sigma–Aldrich, with primary particle sizes of 29 nm (calculated by the Scherrer equation) and BET surface areas around 46 $m^2 g^{-1}$. ^1H, ^{13}C, and ^{119}Sn NMR data were recorded on a Bruker Avance III 500 spectrometer at 500.3, 125.8, and 186.4 MHz, respectively. The spectra were referenced to $SiMe_4$ ($\delta = 0$ ppm for ^1H, ^{13}C) and $SnMe_4$ ($\delta = 0$ ppm for ^{119}Sn). Solid-state NMR measurements were performed at 9.4 T on a Bruker Avance 400 spectrometer equipped with double-tuned probes capable of magic angle spinning (MAS). ^{13}C-{^1H}-CP-MAS NMR spectroscopy was accomplished in 4 mm rotors made of zirconium oxide spinning at 12.5 kHz. Cross-polarization with contact times of 3 ms was used to enhance sensitivity. The recycle delay was 5 s. ^{119}Sn-{^1H}-CP-MAS NMR spectroscopy was performed in 4 mm rotors spinning at 12.5 kHz. The recycle delay was 10 s. All spectra were obtained under ^1H decoupling using a two-pulse phase modulation sequence. The spectra were referenced with respect to tetramethylsilane (TMS) with tetracyclohexylstannane as a secondary standard ($\delta = 3.6$ ppm for ^{13}C, $\delta = -97.3$ ppm for ^{119}Sn). If not stated otherwise, all spectra were acquired at room temperature. Single-crystal X-ray diffraction analyses for compounds **2**, **2a**, and **3** were performed by using an Oxford Gemini S diffractometer with graphite-monochromated CuK_α radiation at 293 (**2**), 160 (**2a**), and 120 K (**3**). The structures were solved by direct methods with SHELXS-97 and refined with SHELXL-97. The figures were created by DIAMOND (version 3.1, 2006). CCDC 854547 (**2**), 854689 (**2a**), 854548 (**3**), and 854549 (calix[4]resorcinarene octamethyl ether) contain the supplementary crystallographic data for this paper. These data can be obtained free of charge from the Cambridge Crystallographic Data centre via www.ccdc.cam.ac.uk/data_request/cif.

Powder X-ray diffraction (PXRD) patterns were measured with a STOE-STADI-P diffractometer using CuK_α radiation (40 kV, 40 mA). The crystallite size was estimated by using the formula determined by the Scherrer equation: $\tau = K\lambda/\beta\cos\theta$, in which τ is the volume-weighted crystallite size in nm, K is the Scherrer constant here taken as 1.0, λ is the X-ray wavelength, θ is the Bragg angle in rad, and β is the full width of the diffraction line at half of the maximum intensity.

Attenuated total reflection–IR spectra were recorded on a Biorad FTS-165 spectrometer with a Spectromat Golden-Gate attachment. Elemental analysis was performed by a Thermo Type Flash AE 1112 elemental analyzer. Thermogravimetric measurements were performed with a PerkinElmer TGA 7 instrument. Specific surface analyses were performed with N_2 adsorption–desorption isotherms at liquid nitrogen temperature (77 K) using a Quantachrome Autosorb IQ2 apparatus, and were evaluated by the Brunauer–Emmett–Teller (BET) method at the p/p_0 ratio of 0.150.

Transmission electron micrographs were obtained by a 200 kV high-resolution transmission electron microscope (CM 20 FEG, Philips) with an imaging energy filter from Gatan (GIF). For the high-angle annular dark-field (HAADF)–scanning electron transmission microscopy (STEM) analysis, the samples (embedded in an epoxy resin) were cut ultrathin by a Leica UCT ultramicrotome and analyzed by an FEI Tecnai F20 field-emission transmission electron microscope. X-ray photoelectron spectroscopy was performed with an Axis Ultra photoelectron spectrometer (Kratos Analytical, UK). The spectrometer was equipped with a monochromatic $AlK_{\alpha 1,2}$ X-ray source operating at 300 W and 20 mA. The kinetic energy of the photoelectrons was determined with a hemispheric analyzer set to a pass energy of 160 eV for the wide-scan spectra and 20 eV for the high-resolution spectra. During all measurements, electrostatic charging of the sample was overcompensated for by means of a low-energy electron source working in combination with a magnetic immersion lens.

Synthesis of the tin monomers

Synthesis of tetra(furan-2-ylmethoxy)stannane (**1**): Furfuryl alcohol (2.67 g, 27.23 mmol) was dropped into an ice-cold solution of tetra-*tert*-butoxystannane (2.78 g, 6.76 mmol) in *n*-pentane (40 mL). After 1 h the precipitate was isolated by filtration and washed with diethyl ether (30 mL). The beige solid was dried in vacuo (10^{-2} mbar, 50 °C) to afford compound **1** (2.68 g, 78 %, m.p. 107 °C). ^{13}C-{^{1}H}-CP-MAS NMR (100.6 MHz): δ = 159.2, 154.1, 142.7, 111.6, 107.8, 58.5 ppm; ^{119}Sn-{^{1}H}-CP-MAS NMR (149.2 MHz): δ = −595, −602 ppm; IR: $\tilde{\nu}$ = 3145/3121 (w), 2929/2865 (w), 1500/1599 (m), 1461/1441 (w), 1365 (m), 1280 (w), 1223/1200 (m), 1444 (s), 1008 (s), 971 (m), 944 (m), 909 (s), 881 (m), 823 (m), 725 (s), 636 (w), 598 (m), 550 cm^{-1} (m); elemental analysis calcd (%) for $C_{20}H_{20}O_8Sn$: C 47.37, H 3.98; found: C 47.34, H 4.73.

Synthesis of bis(μ_2-thiophen-2-ylmethoxy)-hexakis(thiophen-2-ylmethoxy)-bis(thiophen-2-ol)-distannane (**2**): 2-Thiophenemethanol (2.31 g, 20.20 mmol) was dropped into a solution of tetra-*tert*-butoxystannane (1.67 g, 4.05 mmol) in toluene (10 mL). The mixture was stirred for 1 h and the orange solution was covered with *n*-pentane (10 mL) to give large orange crystals of **2** (1.48 g, 53 %, m.p. 100–109 °C). Slow diffusion of moisture into a reaction vessel of **2** in *n*-pentane resulted in the formation of a crop of single crystals of di{(μ_2-hydroxo)-(μ_3-oxido)-tris(μ_2-thiophen-2-ylmethoxy)-hexakis(2-thiophen-2-ylmethoxy)-(thiophen-2-ol)-tristannane)} (**2a**) used for single-crystal X-ray diffraction analysis.

2: ^{1}H NMR (500.3 MHz, $CDCl_3$): δ = 7.31 (br, 2H; OH), 7.19–6.69 (30H; thiophenyl), 5.24 (br, 4H; CH_2), 4.85 (br, 12H; CH_2), 4.70 ppm (br, 4H; CH_2); ^{13}C-{^{1}H} NMR (125.8 MHz, $CDCl_3$): δ = 147.7, 143.1, 142.4, 126.6 (br), 126.3, 126.1, 125.9, 124.2, 124.1, 123.4, 62.1, 61.8, 61.2 ppm; ^{119}Sn-{^{1}H} NMR (186.4 MHz, $CDCl_3$): δ = −623 ppm; IR: $\tilde{\nu}$ = 3099/3078 (w), 2932/2845 (w), 1434 (m), 1366 (m), 1262(w), 1220 (m), 1163 (m), 1002 (s), 932 (s), 831 (s), 748 (w), 690 (s), 540/516 (m), 436 (m), 413 cm^{-1} (m); elemental analysis calcd (%) for $C_{50}H_{52}O_{10}S_{10}Sn_2$: C 43.80, H 3.82, S 23.39; found: C 42.83, H 3.92, S 22.91. **2a**: IR: $\tilde{\nu}$ = 3100/3069 (w), 2934/2859 (w), 1433 (m), 1369 (m), 1265(w), 1217 (m), 1165 (m), 1032 (s), 970 (s), 825 (s), 750 (w), 692 (s), 547/513 (m), 464 (m), 416 cm^{-1} (m); elemental analysis calcd (%) for $C_{103.5}H_{108}O_{24}S_{20}Sn_6$: C 40.24, H 3.52, S 20.76; found: C 40.29, H 4.21, S 21.23.

Synthesis of bis{μ_2-(2-methoxybenzyl)oxy}-hexakis{(2-methoxybenzyl)oxy}-bis{(2-methoxyphenyl)methanol}-distannane (**3**): (2-Methoxyphenyl)methanol (1.16 g, 8.37 mmol) was dropped into a solution of tetra-*tert*-butoxystannane (0.86 g, 2.09 mmol) in *n*-pentane (50 mL) to give a precipitate, which was isolated by filtration after 60 min. The amorphous product was dissolved in toluene (40 mL). The solution was covered with *n*-pentane (10 mL) to give colorless crystals of **3** (0.59 g, 35 %, m.p. 144–148 °C). ^{1}H NMR (500.3 MHz, C_6D_6): δ = 8.58 (br, 2H; OH), 7.65–6.04 (unresolved multiplets, 40H; aryl groups), 5.36 (br, 4H; CH_2), 5.19 (br, 12H; CH_2), 4.69 (br, 4H; CH_2), 3.26–3.12 ppm (br, 30H; OCH_3); ^{13}C-{^{1}H} NMR (125.8 MHz, $CDCl_3$): δ = 54.6, 54.8, 55.2, 62.1 (br), 109.1 (br), 120.1 (br), 127.1 (br), 128.8 (br), 133.1 (br), 155.9, 156.6, 157.5 ppm; ^{119}Sn-{^{1}H} NMR (186.4 MHz, C_6D_6): δ = −622 ppm; IR: $\tilde{\nu}$ = 3066/3005 (w), 2936/2898 (w), 2833 (w), 1588 (m), 1488/1460/1436 (s), 1372 (m), 1282 (m), 1232 (s), 1114 (m), 1021 (s), 928 (m), 813 (w), 744 (s), 712 (m), 666 (m), 610 (m), 580 (w), 521 (m), 482 (m), 435 cm^{-1} (m); elemental analysis calcd (%) for $C_{80}H_{92}O_{20}Sn_2$: C 59.64, H 5.76; found: C 59.34, H 6.13.

Synthesis of bis{μ_2-(2,4-dimethoxybenzyl)oxy}-hexakis{(2,4-dimethoxybenzyl)oxy}-bis{(2,4-dimethoxyphenyl)methanol}-distannane (**4**): Tetra-*tert*-pentyloxystannane (0.5 mL, 1.31 mmol) was dissolved in diethyl ether (15 mL) and cooled to 0 °C. A solution of 2,4-dimethoxybenzyl alcohol (1.77 g, 10.51 mmol) in diethyl ether (15 mL) was dropped into the reaction mixture. The viscous precipitate was washed with diethyl ether until a colorless amorphous solid was formed. The product was dried in vacuo (10^{-2} mbar, 50 °C) to give **4** as a colorless solid (0.44 g, 42 %, m.p. 85–120 °C). ^{1}H NMR (500.3 MHz, $CDCl_3$): δ = 7.99–6.24 (30H; aryl groups), 5.44–4.68 (br, 20H; CH_2), 3.82–3.51 ppm (br, 60H; OCH_3); ^{13}C-{^{1}H} NMR (125.8 MHz, $CDCl_3$): δ = 160.7, 158.7, 156.9, 129.7, 127.8, 121.8, 104.0, 103.7, 98.7, 97.4, 61.7, 54.9, 55.3 ppm; ^{119}Sn-{^{1}H} NMR (186.4 MHz, $CDCl_3$): δ = −623 ppm; IR: $\tilde{\nu}$ = 3081 (w), 2996/2942 (m), 2834 (m), 1610/1587 (m), 1504 (s), 1456 (s), 1282 (s), 1203 (s), 1153 (s), 1020 (m), 1032 (s), 929 (m), 819 (s), 783 (m), 627 (m), 571 (w), 521 (m), 509 (m), 451 cm^{-1} (m); elemental analysis calcd (%) for $C_{90}H_{112}O_{30}Sn_2$: C 56.56, H 5.91; found: C 55.46, H 6.00.

Synthesis of 2,2′-spirobi[4*H*-1,3,2-benzodioxastannine] (**5**): 2-(Hydroxymethyl)phenol (0.74 g, 5.94 mmol) was added to a solution of tetra-*tert*-butoxystannane (1.22 g, 2.97 mmol) in toluene (10 mL). The reaction mixture was heated to 110 °C and *tert*-butyl alcohol was removed by distillation to give a precipitate that was isolated by filtration and washed with toluene. The light yellow solid was dried in vacuo (10^{-2} mbar, 50 °C) to afford compound **5** (0.83 g, 77 %, decomposed at 250 °C). ^{13}C-{^{1}H}-CP-MAS NMR (100.6 MHz): δ = 71.4, 120.9, 127.6, 159.7 ppm; ^{119}Sn-{^{1}H}-CP-MAS NMR (149.2 MHz): δ = −697 ppm; IR: $\tilde{\nu}$ = 3063 (w), 3028 (w), 2917 (w), 2870 (w), 1599 (m), 1479 (s), 1450 (s), 1254 (s), 1223 (s), 1196 (s), 1109 (m), 931 (s), 875 (m), 752 (s), 727 (s), 621 (s), 513 (s), 457 (m), 412 cm^{-1} (m); elemental analysis calcd (%) for $C_{14}H_{12}O_4Sn$: C 46.33, H 3.33; found: C 46.45, H 3.87.

Synthesis of 2,2′-spirobi[6-methylbenzo(4*H*-1,3,2)dioxastannine] (**6**): A solution of 2-(hydroxymethyl)-4-methylphenol (1.64 g, 11.90 mmol) in diethyl ether (20 mL) was added to a solution of tetra-*tert*-butoxystannane (2.23 g, 5.41 mmol) in diethyl ether (10 mL). After stirring for 2 h the precipitate was isolated by filtration and washed with *n*-pentane (30 mL). The yellow solid was dried in vacuo (10^{-2} mbar, 50 °C) to afford compound **6** (1.54 g, 73 %, decomposed at 210 °C). ^{1}H NMR (500.3 MHz, $CDCl_3$): δ = 6.93 (br, 6H; aryl groups), 4.59 (br, 4H; CH_2), 2.26 ppm (br, 6H; CH_3); ^{13}C-{^{1}H}-CP-MAS NMR (100.6 MHz): δ = 19.8, 72.2, 121.2, 129.0, 157.9 ppm; ^{119}Sn-{^{1}H}-CP-MAS NMR (149.2 MHz): δ = −705 ppm; IR: $\tilde{\nu}$ = 3011 (w), 2918 (w), 2861 (w), 1610 (w), 1488 (s), 1462 (s), 1375 (w), 1146 (m), 1124 (m), 985 (m), 869 (w), 798 (s), 662 (w), 499 (s), 416 cm^{-1} (m); elemental analysis calcd (%) for $C_{16}H_{16}O_4Sn$: C 49.15, H 4.12; found: C 49.50, H 4.49.

Synthesis of 2,2′-spirobi[6-methoxybenzo(4*H*-1,3,2)dioxastannine] (**7**): A solution of tetra-*tert*-butoxystannane (1.23 g, 2.99 mmol) in tetrahydrofuran (20 mL) was dropped into a solution of 2-(hydroxymethyl)-4-methoxyphenol (1.15 g, 7.47 mmol) in tetrahydrofuran (20 mL) at −60 °C. The colorless mixture was stirred for 30 min at −60 °C and 30 min at room temperature. Tetrahydrofuran was removed and the viscous yellow crude product was washed with *n*-pentane (50 mL) and diethyl ether (50 mL). The pale yellow solid was dried in vacuo (10^{-2} mbar, 50 °C) to afford compound **7** (1.13 g, 90%, decomposed at 240 °C). ^{1}H NMR (500.3 MHz, $CDCl_3$): $\delta = 6.79$ (br, 6H; aryl groups), 4.67 (br, 4H; CH_2), 3.74 ppm (br, 6H; OCH_3); ^{13}C-{^{1}H}-CP-MAS NMR (100.6 MHz): $\delta = 54.9$, 72.3, 110.9, 118.2, 126.5, 153.6 ppm; ^{119}Sn-{^{1}H}-CP-MAS NMR (149.2 MHz): $\delta = -683$ ppm; IR: $\tilde{\nu} = 2938$ (w), 2832 (w), 1599 (w), 1485 (s), 1423 (m), 1248 (m), 1203 (s), 1153 (m), 1037 (m), 960 (m), 918 (m), 852(m), 794 (s), 785 (s), 719 (m), 669 (m), 571 (s), 503 cm^{-1} (s); elemental analysis calcd (%) for $C_{16}H_{16}O_6Sn$: C 45.43, H 3.81; found: C 45.13, H 4.10.

Cationic polymerization

Polymerization in melt: Compound **1** was heated to 120 °C for 3 h under inert conditions. The resulting dark brown composite was extracted with dichloromethane until the extracts were colorless and dried in vacuo to constant weight.

Heat treatment: Compound **5** and 4-methylbenzenesulfonic acid were suspended in toluene. After stirring for a few minutes, the solvent was removed and the reaction mixture was heated to 280 °C for 15 min under argon. The dark red composite material was washed with chloroform and acetone and dried at 70 °C.

Polymerization in solution: The tin monomers were dissolved at room temperature in dry chloroform (0.1 mol L^{-1}) under an argon atmosphere. The initiator (M:I, see Table 2) dissolved in chloroform was added dropwise. The composite material was isolated by filtration, extracted with dichloromethane, and dried in vacuo.

Simultaneous twin polymerization

Compound **5** (1.02 g, 3.74 mmol) was suspended in a solution of 2,2′-spirobi[4*H*-1,3,2-benzodioxasiline] (0.68 g, 1.87 mmol) in dry chloroform (10 mL) at a Si/Sn ratio of 2:1. After stirring for a few minutes, the solvent was removed and the reaction mixture was heated slowly to 80 °C for half an hour. The brown composite material was washed with acetone and dried at 70 °C.

2,2′-Spirobi[4*H*-1,3,2-benzodioxasiline] (0.9 g, 3.30 mmol) and compound **6** (0.65 g, 1.65 mmol) or **7** (0.59 g, 1.65 mmol) were dissolved in dry chloroform (10 mL) at a Si/Sn ratio of 2:1. The solvent was removed after stirring for a few minutes and the mixture was heated slowly to 100 °C for half an hour. The yellow composites were washed with acetone and dried at 70 °C.

Oxidation reactions

The removal of the organic polymeric material by oxidation was performed in a tube furnace. The composite was treated with a constant airstream (200 L h^{-1}) to give a light beige solid of SnO_2. The oxidation conditions are given in Tables 3 and 5.

Acknowledgements

We thank Prof. Dr. S. Spange for fruitful discussions. We are grateful to the BASF Aktiengesellschaft Ludwigshafen and the Deutsche Forschungsgemeinschaft (FOR 1497) for financial support.

Keywords: nanoparticles · NMR spectroscopy · organic–inorganic hybrid materials · tin alkoxides · twin polymerization

[1] G. Faglia, C. Baratto, G. Sberveglieri, M. Zha, A. Zappettini, *Appl. Phys. Lett.* **2005**, *86*, 011923.
[2] M. Fuchs, D. Breitenstein, M. Fartmann, T. Grehl, S. Kayser, R. Koester, R. Ochs, S. Schlabach, D. V. Szabóa, M. Brunsa, *Surf. Interface Anal.* **2010**, *42*, 1131.
[3] K. Yao, D. Caruntu, B. Cao, C. J. O'Connor, W. Zhou, *IEEE Trans. Nanotechnol.* **2010**, *9*, 630.
[4] B. Schumacher, R. Ochs, H. Tröße, S. Schlabach, M. Bruns, D. V. Szabó, J. Haußelt, *Plasma Processes Polym.* **2007**, *4*, S865.
[5] C.-D. Kohl, A. Eberheim, P. Schieberle, *Tech. Mess.* **2004**, *71*, 298.
[6] J. Watson, K. Ihokura, G. Coles, *Meas. Sci. Technol.* **1993**, *4*, 711.
[7] Y.-D. Wang, C.-L. Ma, X.-H. Wu, X.-D. Sun, H.-D. Li, *Talanta* **2002**, *57*, 875.
[8] M. Ando, S. Suto, T. Suzuki, T. Tsuchida, C. Nakayama, N. Miura, N. Yamazoe, *J. Ceram. Soc. Jpn.* **1996**, *104*, 409.
[9] W. Göpel, J. Hesse, J. N. Zemel, in *Chemical and Biochemical Sensors, Vol. 2*, VCH Weinheim, New York, **1991**.
[10] T. Stergiopoulos, I. M. Arabatzis, H. Cachet, P. Falaras, *J. Photochem. Photobiol. A* **2003**, *155*, 163.
[11] D. Niles, D. Rioux, H. Höchst, *J. Appl. Phys.* **1993**, *73*, 4586.
[12] G. Frank, E. Kauer, H. Köstlin, F.-J. Schmitte, *Proc. Soc. Photo-Opt. Instrum. Eng.* **1982**, *324*, 58.
[13] K. Yu, Z. C. Wu, Q. R. Zhao, B. X. Li, Y. Xie, *J. Phys. Chem. C* **2008**, *112*, 2244.
[14] Y. Wang, J. Y. Lee, *J. Phys. Chem. B* **2004**, *108*, 17832.
[15] M. Mohamedi, S.-J. Lee, D. Takahashi, M. Nishizawa, T. Itoh, I. Uchida, *Electrochim. Acta* **2001**, *46*, 1161.
[16] G.-L. Xu, S.-R. Chen, J.-T. Li, F.-S. Ke, L. Huang, S.-G. Sun, *J. Electroanal. Chem.* **2011**, *656*, 185.
[17] K. E. Aifantis, S. Brutti, S. A. Hackneya, T. Sarakonsria, B. Scrosatie, *Electrochim. Acta* **2010**, *55*, 5071.
[18] L. Cuia, J. Shena, F. Chenga, Z. Taoa, J. Chena, *J. Power Sources* **2011**, *196*, 2195.
[19] X. Yin, L. Chen, C. Li, Q. Hao, S. Liu, Q. Li, E. Zhang, T. Wang, *Electrochim. Acta* **2011**, *56*, 2358.
[20] T. Prem Kumar, R. Ramesh, Y. Y. Lin, G. Ting-Kuo Fey, *Electrochem. Commun.* **2004**, *6*, 520.
[21] A. Yu, R. Frech, *J. Power Sources* **2002**, *104*, 97.
[22] M. Dimitrov, T. Tsoncheva, S. Shao, R. Köhn, *Appl. Catal. B* **2010**, *94*, 158.
[23] T.-Y. Wei, C.-Y. Kuo, Y.-J. Hsu, S.-Y. Lu, Y.-C. Chang, *Microporous Mesoporous Mater.* **2008**, *112*, 580.
[24] A. P. Rizzato, C. V. Santilli, S. H. Pulcinelli, P. Hammera, V. Briois, *J. Eur. Ceram. Soc.* **2005**, *25*, 2045.
[25] L. R. B. Santos, T. Chartier, C. Pagnoux, J. F. Baumarda, C. V. Santillii, S. H. Pulcinelli, A. Larbot, *J. Eur. Ceram. Soc.* **2004**, *24*, 3713.
[26] S. Belin, L. R. B. Santos, V. Briois, A. Lusvardi, C. V. Santilli, S. H. Pulcinelli, T. Chartier, A. Larbot, *Colloids Surf. A* **2003**, *216*, 195.
[27] S. de Monredon, A. Cellot, F. Ribot, C. Sanchez, L. Armelao, L. Gueneau, L. Delattre, *J. Mater. Chem.* **2002**, *12*, 2396.
[28] A. Hagemeyer, Z. Hogan, M. Schlichter, B. Smaka, G. Streukens, H. Turner, A. Volpe, H. Weinberg, K. Yaccato, *Appl. Catal. A* **2007**, *317*, 139.
[29] J. A. Toledo-Antonio, R. Gutiérrez-Baez, P. J. Sebastian, A. Vázquez, *J. Solid State Chem.* **2003**, *174*, 241.
[30] Z. Li, Z. Wang, X. Xiang, X. Zu, L. Wei, L. Wang, *J. Sol-Gel Sci. Technol.* **2009**, *49*, 196.
[31] J. Zhu, B. Y. Tay, J. Ma, *J. Mater. Process. Techol.* **2007**, *192–193*, 561.
[32] Y. D. Wang, C. L. Mab, H. D. Li, S. Zhang, *Mater. Chem. Phys.* **2008**, *107*, 248.
[33] S. Supothina, M. R. De Guire, *Thin Solid Films* **2000**, *371*, 1.

[34] F. Chen, M. Liu, *Chem. Commun.* **1999**, 1829 – 1830.
[35] K. G. Severin, T. M. Abdel-Fattah, T. J. Pinnavaia, *Chem. Commun.* **1998**, 1471 – 1472.
[36] E. A. Gulliver, J. W. Garvey, T. A. Wark, M.-J. Hampden-Smith, A. Datyet, *J. Am. Ceram. Soc.* **1991**, *74*, 1091.
[37] Z. P. Guo, G. D. Du, Y. Nuli, M. F. Hassan, H. K. Liu, *J. Mater. Chem.* **2009**, *19*, 3253.
[38] H. Huang, E. M. Kelder, L. Chen, J. Schoonman, *Solid State Ionics* **1999**, *120*, 205.
[39] M. Niederberger, G. Garnweitner, *Chem. Eur. J.* **2006**, *12*, 7282.
[40] J. Ba, J. Polleux, M. Antonietti, M. Niederberger, *Adv. Mater.* **2005**, *17*, 2509.
[41] N. Pinna, G. Neri, M. Antonietti, M. Niederberger, *Angew. Chem.* **2004**, *116*, 4445; *Angew. Chem. Int. Ed.* **2004**, *43*, 4345.
[42] A. Aboulaich, B. Boury, P. H. Mutin, *Eur. J. Inorg. Chem.* **2011**, 3644.
[43] S. Grund, S. Spange, *Adv. Mater.* **2009**, *21*, 2111.
[44] S. Spange, P. Kempe, A. Seifert, A. Auer, P. Ecorchard, H. Lang, M. Falke, M. Hietschold, A. Pohlers, W. Hoyer, G. Cox, E. Kockrick, S. Kaskel, *Angew. Chem.* **2009**, *121*, 8403; *Angew. Chem. Int. Ed.* **2009**, *48*, 8254.
[45] A. Mehner, T. Rüffer, H. Lang, A. Pohlers, W. Hoyer, S. Spange, *Adv. Mater.* **2008**, *20*, 4113.
[46] F. Böttger-Hiller, R. Lungwitz, A. Seifert, M. Hietschold, M. Schlesinger, M. Mehring, S. Spange, *Angew. Chem.* **2009**, *121*, 9039; *Angew. Chem. Int. Ed.* **2009**, *48*, 8878.
[47] A. A. Auer, A. Richter, A. V. Berezkin, D. V. Guseva, S. Spange, *Macromol. Theory Simul.* **2012**, *21*, 615.
[48] T. Löschner, A. Mehner, S. Grund, A. Seifert, A. Pohlers, A. Lange, G. Cox, H. J. Hähnle, S. Spange, *Angew. Chem.* **2012**, *124*, 3312; *Angew. Chem. Int. Ed.* **2012**, *51*, 3258; *Angew. Chem.* **2012**, *124*, 3312.
[49] M. J. Hampden-Smith, T. A. Wark, *Can. J. Chem.* **1991**, *69*, 121.
[50] H. Reuter, M. Kremser, *Z. Anorg. Allg. Chem.* **1992**, *615*, 137.
[51] Z. Lin, J. Rocha, J. D. Pedrosa de Jesus, A. Ferreira, *J. Mater. Chem.* **2000**, *10*, 1353.
[52] A. Navío, M. Macias, G. Colón, P. J. Sánchez-Soto, V. Augugliaro, L. Palmisano, *Appl. Surf. Sci.* **1994**, *81*, 325.
[53] N. K. Mal, V. Ramaswamy, S. Ganapathy, A. V. Ramaswamy, *Appl. Catal. A* **1995**, *125*, 233.
[54] Y. S. Avadhut, J. Weber, E. Hammarberg, C. Feldmann, I. Schellenberg, R. Pöttgen, J. Schmedt auf der Günne, *Chem. Mater.* **2011**, *23*, 1526.
[55] S. Grund, P. Kempe, G. Baumann, A. Seifert, S. Spange, *Angew. Chem.* **2007**, *119*, 636; *Angew. Chem. Int. Ed.* **2007**, *46*, 628; *Angew. Chem.* **2007**, *119*, 636.
[56] H. Pasch, P. Goetzky, E. Gründemann, H. Raubach, *Acta. Polym.* **1981**, *32*, 14.
[57] B. Ottenbourgs, P. Adriaensens, R. Carleer, D. Vanderzande, J. Gelan, *Polymer* **1998**, *39*, 5293.
[58] B. Park, B. Riedl, *J. Appl. Polym. Sci.* **2000**, *77*, 841.
[59] E. W. Corcoran, Jr., D. E. W. Vaughan, *Solid State Ionics* **1989**, *32 – 33*, 423 – 429.
[60] A. Dyer, J. J. Jafar, *J. Chem. Soc. Dalton Trans.* **1990**, 3239.
[61] S. K. Song, W. K. Choi, H. J. Jung, H. K. Baik, S. K. Koh, *Nanostruct. Mater.* **1997**, *8*, 477.
[62] M. H. Kibel, P. W. Leech, *Surf. Interface Anal.* **1996**, *24*, 605.
[63] J. Finster, E. D. Klinkenberg, J. Heeg, W. Braun, *Vacuum* **1990**, *41*, 1586.
[64] K. S. W. Sing, D. H. Everett, R. A. W. Haul, L. Moscou, R. A. Pierotti, J. Rouquerol, L. Siemieniewska, *Pure Appl. Chem.* **1985**, *57*, 603.
[65] S. G. Gregg, K. S. W. Sing, *Adsorption, Surface Area and Porosity*, Academic Press, San Diego, **1982**.
[66] F. L. Chen, Z. Shi, M. L. Liu, *Chem. Commun.* **2000**, 2095.
[67] T. T. Van Tran, T. S. Bui, S. Turrell, B. Capoen, P. Roussel, M. Bouazaoui, M. Ferrari, O. Cristini, C. Kinowski, *J. Raman Spectrosc.* **2012**, *43*, 869.
[68] Y. S. Feng, S. M. Zhou, Y. Li, L. D. Zhang, *Mater. Lett.* **2003**, *57*, 2409.
[69] O. Morikawa, E. Iyama, T. Oikawa, K. Kobayashi, H. Konishi, *J. Phys. Org. Chem.* **2006**, *19*, 214.

Received: September 13, 2012
Revised: August 14, 2013
Published online on ■■ ▮▮, 0000

*C. Leonhardt, S. Brumm, A. Seifert, G. Cox, A. Lange, T. Rüffer, D. Schaarschmidt, H. Lang, N. Jöhrmann, M. Hietschold, F. Simon, M. Mehring**

■■ – ■■

Tin Oxide Nanoparticles and SnO_2/SiO_2 Hybrid Materials by Twin Polymerization Using Tin(IV) Alkoxides

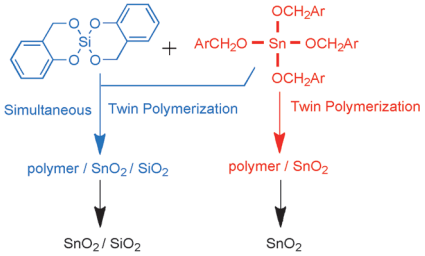

Double act: Well-defined tin alkoxide precursors have been prepared for application in the twin polymerization process, which provides composite materials composed of SnO_2 nanoparticles entrapped in a polymer matrix (see scheme). Subsequent oxidation of the composite materials gives high-surface-area tin oxide and composites composed of SnO_2/SiO_2.